Passive hyperspectral terahertz imagery for security screening using a cryogenic microbolometer*

Arttu Luukanen†‡, Aaron J. Miller, and Erich N. Grossman
National Institute of Standards and Technology, Quantum Electrical Metrology Division
325 Broadway, Boulder, CO 80305, U.S.A

ABSTRACT

We present passive indoor imagery of human subjects in the 100 – 1000 GHz band. In order to obtain adequate sensitivity, a cryogenically cooled (4 K), broadband antenna-coupled, superconducting microbolometer with optical noise equivalent power NEP < 2 $pW/Hz^{1/2}$ was used as the sensor. Mechanical scanning of the collecting aperture, a 30 cm diameter spherical mirror, was used to slowly accumulate the images. While not yet practical for deployable real-time cameras, this system provides valuable phenomenological comparisons with similar imagery obtained with actively illuminated systems.

Keywords: bolometer, submillimeter-wave, superconducting

1. Introduction

Passive detection and identification of concealed threat items using millimeter or submillimeter waves is a daunting task, especially if the imaging is done indoors, due to the small radiometric temperature contrasts between the (hidden) target objects and the human body. The typical signal levels are of the order of a few picowatts, requiring either very sensitive detectors or alternatively active illumination. For passive detection, a Noise Equivalent Temperature Difference (NETD) of less than 1 K is required. In order to reach subkelvin NETD, a detector with a low noise equivalent power (NEP) and a large predetection bandwidth is needed.

2. Description of the sensor

The antenna-coupled microbolometer consists of a lithographic antenna coupled to a microscopic, thermally isolated RF termination–the bolometer. Incident radiation is coupled to the bolometer, and the resulting temperature rise can be sensed by passing a DC current through (or by applying a DC voltage across) the device, and measuring the voltage (or current) change. At room temperature, the sensitivity of metallic microbolometers is poor due to the small temperature coefficient of resistance of metals, which is typically 0.1 %/K - 0.3 %/K. However, if the metallic device is cooled, the sensitivity or the noise equivalent power can be improved through a reduction in the thermal noise. In the most extreme case, a superconducting bolometer film can be voltage-biased within its superconductor-normal metal transition, where the temperature coefficient of resistance is typically larger than 1000 %/K.

The antenna in our case is a logarithmic spiral on Si with a design bandwidth from 75 GHz to 1200 GHz, and a feed-point impedance of 75 Ω. The bolometer is a 36 μm x 1 μm x 50 nm film of Nb. The bolometer is suspended from its ends in vacuum to maximize its thermal isolation from the heat bath (the substrate). This helps in obtaining large current responsivity, and reduces the most fundamental noise source for bolometers, namely the phonon noise that originates from energy fluctuations between the heat bath and the bolometer across the thermal conductance $G \equiv dP/dT$.

2.1. Superconducting vacuum-bridge hot-spot bolometer

The operating principle of this detector has been presented in Refs. 1 & 2 and will be discussed only briefly here. In short, the device is connected to a bias circuit that consists of the series combination of the bolometer and a current

† luukanen@boulder.nist.gov; (303) 497-4590; fax (303) 497-3042

‡ on leave from VTT Information Technology, Espoo, Finland

sensing resistor R_L (10 Ω in our case), connected in parallel with a shunt resistor R_s (also 10 Ω). The shunt resistor provides an effective voltage source for the detector-sensing resistor combination as long as the resistance of the bolometer $R_b >> R_s$. The use of a voltage bias is a very convenient way of biasing transition-edge sensors, as this makes the biasing point inherently stable due to a strong negative electrothermal feedback (ETF) that maintains the operating point within the transition [3]. The use of a current bias on the other hand makes stable biasing very difficult, due to the strong positive electrothermal feedback. Most importantly for a voltage bias, the bolometer is essentially immune to even large fluctuations in the bath temperature, since the bridge has a critical temperature T_c (≈ 9 K) well above the bath temperature T_0 (4 K), and the heat flow to the bath is proportional to T_c^2-T_0^2 in the case of Wiedemann-Franz law limited thermal conductance. When the bias is sufficient that the current delivered by the bias circuit to the bolometer exceeds the critical current, the bridge switches to the normal state. As the bias voltage is reduced, the approximately quadratic temperature gradient in the bridge causes the ends of the bridge to cool first below T_c and turn superconducting, while the center portion remains dissipative. This is the operating regime of the detector, where the bias dissipation remains a constant given by $P_b=(T_c-T_o)G$. While the DC resistance of the bridge varies with the bias point, its impedance for the incoming RF remains approximately constant at 75 Ω due to the fact that the detected frequencies are close to or above the superconducting gap frequency. The negative electrothermal feedback maintains the total dissipated power $P_{tot} = P_b+P_{opt}$ fixed, and an increase in the optical power is sensed as a reduction in the current passing through the device.

The NEP of the bolometer is a combination of thermal fluctuation noise (TFN; also known as phonon noise) across the thermal link connecting the bridge to the heat bath, Johnson noise due to its resistance, and amplifier noise. The total electrical NEP of the hot-spot detector is given by

$$\mathrm{NEP} = \left[4\gamma k_B T_c^2 G + \left(\frac{k_B T_c}{R_b} + i_{amp}^2\right)\frac{(1+\beta)^2 V_b{}^2}{L^2}\right]^{1/2}; \qquad (1)$$

γ=0.67 describes the effect of the temperature gradient in the bridge on the TFN[4]. The effect of the bias circuit on the bolometer is given by $\beta = (R_b-R_s)/(R_b+R_s)$. The ETF is characterized by a loop gain $L=[GR_N(T_c-T_0)/(6V^2-GR_N(T_c-T_0)/9)]$, where R_N is the normal state resistance of the bridge. In the optimized case, the NEP is limited by the TFN.

2.2. Detector fabrication

The detectors were fabricated in the NIST Quantum Electrical Metrology Division's cleanroom facility by use of a wafer-scale process. The substrate is a 75 mm diameter 250 μm thick high resistivity wafer (ρ > 5000 Ωcm). First, 50 nm thermal oxide is grown on the substrate using a standard wet oxidation, followed by DC magnetron sputtering of the Nb bolometer layer (50 nm), followed insitu by the antenna metallization (200 nm of Al). The first step of lithography is carried out using a 1 μm thick photoresist that is exposed in a stepper capable of ~0.5 μm resolution. The patterned photoresist is then used as the mask for the Al etch, a commercial Al wet etchant (Transene type A)[5]. A second mask is used after this to define the bolometer strip in a SF_6 dry reactive-ion etch (RIE). A third mask is used to define the etch windows in the SiO_2 on both sides of the bolometer, and another RIE etch is used to etch the SiO_2 down to the Si. Next, the wafer is diced to 6.35 mm x 6.35 mm dies, and the photoresist is left to protect the Nb from the top in the final processing step, where XeF_2 gas-phase etch is used to remove ~2 μm of Si from underneath the Nb bridge. Finally, a O_2 RIE plasma ash is used to remove the protective photoresist. The final result is shown in the SEM images in
Fig. 1.

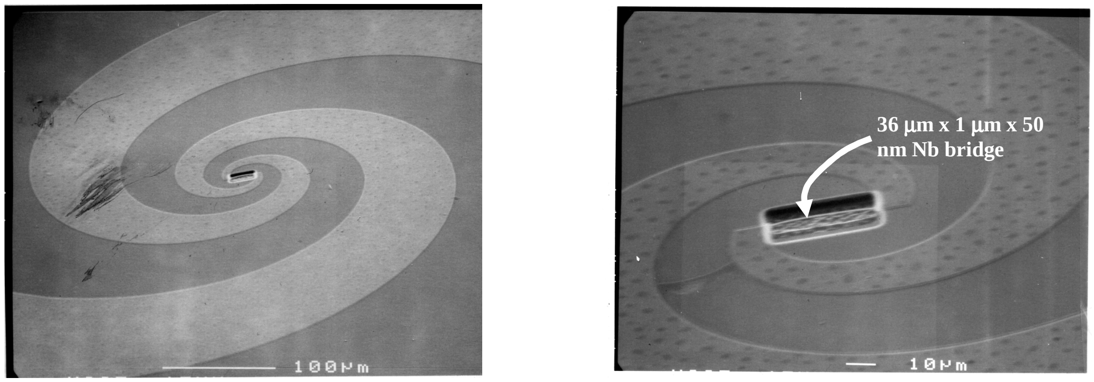

Fig. 1: (Left) A SEM micrograph of the bolometer and the antenna. (Right) A close-up showing the released Nb bridge.

3. Bolometer electrical characterization

The bolometer was electrically characterized after cooling the detector to 4 K in a dewar with no incident radiation. The measured *I-V* curve of the device is shown in Fig. 2. From the *I-V* curve, important parameters such as R_N**,** G, and the electrical responsivity S_I can be determined. Fig. 2 shows the measured *I-V* curve for the device. The *V-P* curve of Fig.2 can be used to determine the $G = P_b/(T_c\text{-}T_0)$ = 3 nW/K. This thermal conductance corresponds to a phonon noise limited NEP ≈ $4\cdot10^{-15}$ W/Hz$^{1/2}$. This is comparable to the 300 K blackbody photon noise limited $NEP_\nu = h\nu(\Delta\nu)^{1/2}(2n_0+n_0^2)^{1/2}$ = $4\cdot10^{-15}$ W/Hz$^{1/2}$, where $h = 6.626\cdot10^{-34}$ J·s is the Planck constant, ν = 450 GHz (center frequency), $\Delta\nu$ = 900 GHz (nominal bandwidth of the antenna), and $n_0 = (e^{h\nu/kT}\text{-}1)^{-1} \approx 13$ is the mean photon occupancy number for a 300 K blackbody.

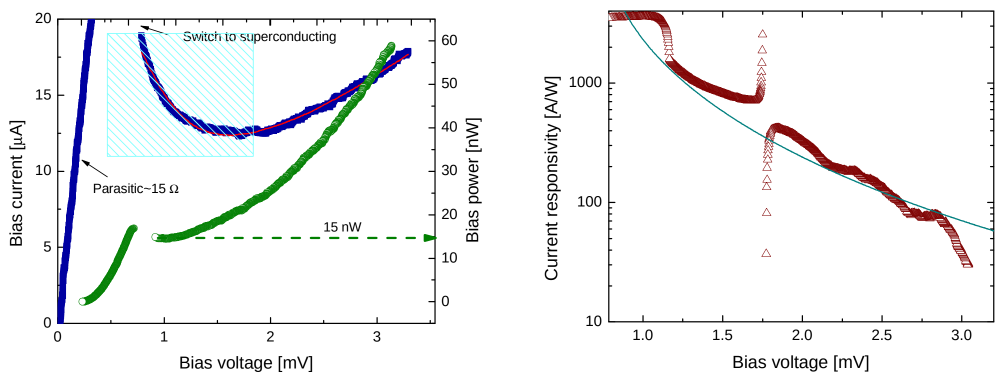

Fig. 2: (Left) The *I-V* curve of the superconducting bolometer. The operating region is where d*I*/d*V* is negative (shaded box). The right axis shows the bias dissipation in the bolometer as a function of the bias voltage. The bias power remains approximately constant within the operating region. (Right) The current responsivity of the bolometer. The solid line indicates the calculated responsivity from the bolometer model. The divergence at ~1.75 mV is a result of dV/dI→∞ near this bias.

4. Optical measurements

For the optical measurements the detector chip was mounted on a 4 mm diameter hyperhemispherical Si lens. First, the beam patterns of the bolometer were measured at room temperature by current biasing the detector and utilizing the fact that the bolometer has responsivity also when operated at room temperature. The combination of detector and Si lens was then mounted on a motorized azimuth-elevation scanning stage with the broadside direction pointing towards a Gunn oscillator 40 cm away. The Gunn output was modulated at 100 Hz, and the detected signal was connected through a low-noise preamplifier to a lock-in amplifier. The beam patterns of the nominally circularly polarized bolometer were measured at two frequencies, 95 GHz and 130 GHz, with the measured amplitude patterns shown in Fig. 3. The 3 dB full widths of the 95 GHz pattern were 41°and 48° in elevation and azimuth, respectively. At 130 GHz, the widths measured 49° in elevation and 45° in azimuth.

For the cryogenic optical measurements, the lens-detector chip assembly was mounted on the 4 K stage of a liquid He dewar equipped with a Teflon window. A heat-sunk fluorogold low-pass filter (cut-off at 1 THz) was mounted at the 4 K shield in the optical path. The first issue of concern was to make sure that our infrared rejection was good enough, as the detector might have some residual response at short wavelengths where there are orders of magnitude more power available. The sufficient high-frequency rejection was confirmed by observation of linear response of the device with blackbody temperature. This was measured by focusing the bolometer beam to a spot smaller than the 9 mm diameter exit aperture of a commercial blackbody cavity with a tunable temperature.
Next, the optical response to a 77 K blackbody placed in front of the window was measured as a function of the bias voltage. While we are still in the process of determining the optical coupling efficiency accurately, Fig. 4 shows that the qualitative agreement between the measured optical signal and that calculated from the *I-V* curve is very good, proving that the coupling efficiency does not change with the biasing point. At this point we estimate the overall optical coupling efficiency referenced to the forward hemisphere of the detector to be ~30 %.
The very low thermal mass of the bolometer makes it very fast. The time constant of the bolometer was determined using a pulsed 100 GHz IMPATT oscillator. The 100 ns pulse response of the device was fitted with an exponential decay of 25 μs.

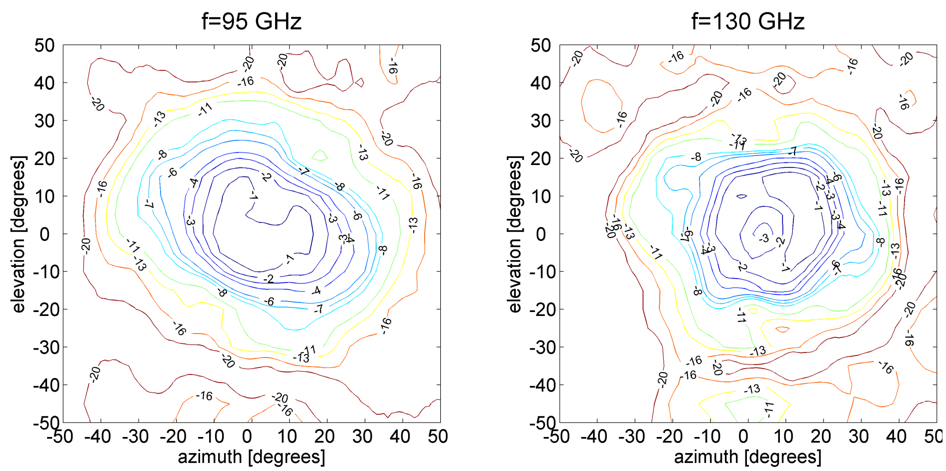

Fig. 3: The amplitude patterns of the log-spiral antenna-coupled microbolometer at 95 GHz (left) and at 130 GHz (right) measured at room temperature using a Gunn oscillator as the source. The contour levels are in dB referenced to the maximum signal.

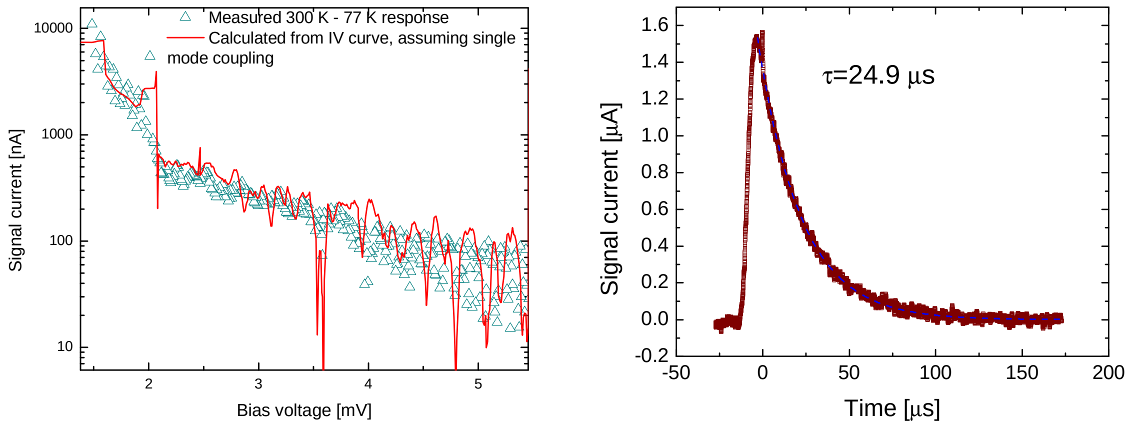

Fig. 4: (Left) The optical response of the detector observing a 77 K blackbody as a function of the bias voltage. The solid line indicates the expected signal current using $I_{sig} = k_B \Delta T \Delta f S_I$, where ΔT = 223 K and Δf = 900 GHz, and the current responsivity $S_I = -[L(1+\beta)/(1+L\beta)V_b]$ in the notation of Eq. (1). (Right) The detector response to a 100 ns pulse from a 100 GHz IMPATT oscillator. The time constant of the detector is ~25 μs.

5. Imagery

The imagery was obtained indoors in a non-controlled environment with no known other sources of illumination at our test bandwidth. The imaging setup is shown in Fig. 5. The main aperture was a 30 cm diameter spherical mirror with a focal length of 25 cm. A double-convex PTFE lens was used to match the f-number of the detector to that of the main aperture. An absorptive chopper was placed at the focus of the lens. The images were obtained by scanning the main aperture in azimuth and elevation. The integration time was 100 ms per pixel for all the images. The responsivity that can be achieved is presently limited by the series resistance R_L, and all the images shown below were collected at a low responsivity of ~ 100 A/W. For measurements at this responsivity the NEP ~ 2 pW/Hz$^{1/2}$ is limited by the 170 pA/Hz$^{1/2}$ current noise of the preamplifier. In the imagery, we estimate 0.3 K < NETD < 0.5 K simply by evaluating the RMS variation in pixels known to be free of signal. Threat items, such as a zirconium oxide kitchen knife and a small handgun were hidden under two cotton shirts, and yielded clear signatures.

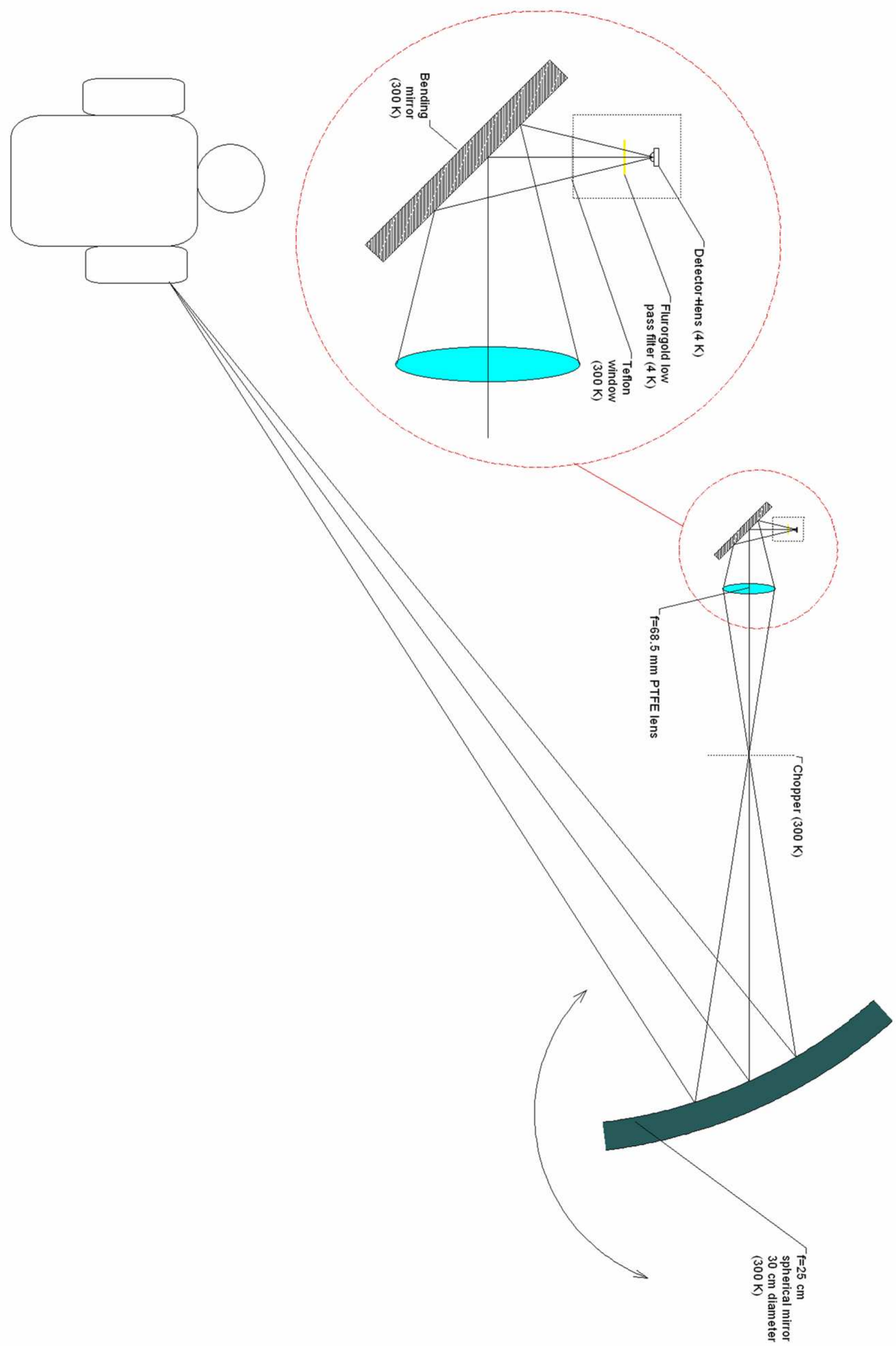

Fig. 5: The configuration of the optics in the imaging experiments (to scale).

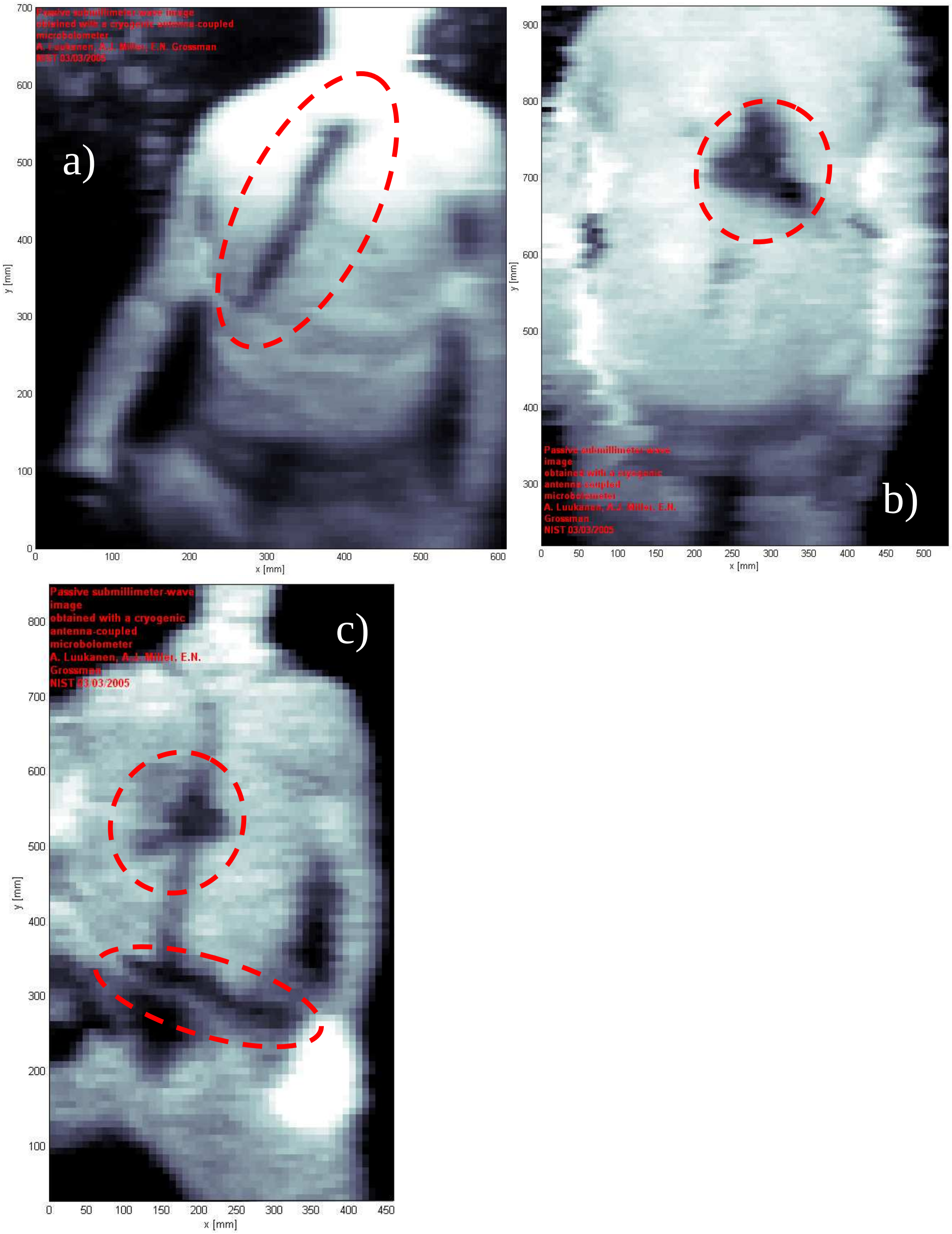

Fig. 6: Passive images in the 100 GHz to 1 THz band. Integration time per pixel was 100 ms, and the scanning of each image took about 30 minutes. The ceramic knife is circled with an oval, while the gun is marked by the circles. The items were hidden under two cotton shirts.

6. Conclusions

We have presented truly passive indoor imagery obtained by a cryogenic antenna-coupled microbolometer coupled to a conventional room temperature amplifier. The detectors have been fabricated on a wafer-scale process that allows future arraying of the detectors. Already with a modest optical NEP of 2 pW/Hz$^{1/2}$ we have shown that NETDs well below 1 K can be reached. The noise is limited by the noise of our preamplifier, and with immediately applicable, straightforward improvements we can improve the NEP to 0.2 pW/Hz$^{1/2}$ (corresponding to a NETD = 30 mK for 100 ms integration time). Work is underway to couple the detector to a superconducting quantum interference device (SQUID) amplifier with a current noise of ~1 pA/Hz$^{1/2}$. This will enable us to reach truly background limited NEP of 4 fW/Hz$^{1/2}$, or a NETD $\leq$ 1 mK. Along with the improvements to the detector sensitivity, we are building a circular variable filter based on frequency-selective surfaces that will be used to sweep a pass-band through the 900 GHz bandwidth of the detector with a spectral resolution of ~10 % around the center frequency. This will enable us to collect important phenomenology of materials signatures for possible identification of hazardous materials.

ACKNOWLEDGEMENTS

The authors thank Sae Woo Nam, Robert Hadfield, Panu Helistö, Mikko Kiviranta, and Leif Grönberg for useful discussions.

---

[1] A. Luukanen and J.P. Pekola, “A superconducting antenna-coupled hot-spot microbolometer”, *Appl. Phys. Lett.* **82**, pp.3970-3972 (2003)

[2] A. Luukanen, R. H. Hadfield, A. J. Miller, E. N. Grossman, “A superconducting antenna-coupled microbolometer for THz applications”, Proc. SPIE Vol. 5411, p. 121-126, Terahertz for Military and Security Applications II; R. Jennifer Hwu, Dwight L. Woolard; Eds.

[3] K.D. Irwin, “An application of electrothermal feedback for high resolution cryogenic particle detection”, *Appl. Phys. Lett.,* **66**, pp.1998-2000 (1998).

[4] J. C. Mather, “Bolometer noise: non-equilibrium theory,” Appl. Opt.,vol. 21, pp. 1125–1129, March 1982.

[5] Products or companies named here are cited only in the interest of complete scientific description, and neither constitute nor imply endorsement by NIST or by the US government. Other products may be found to serve just as well.